Vertical integration of a GaAs/AlGaAs quantum-well laser and a long-wavelength quantum-well infra-red photodetector

J.S. Tsang, C.P. Lee, K.L. Tsai and H.R. Chen

Indexing terms: Integrated optoelectronics, Semiconductor lasers, Infrared detectors, Photodetectors

A short-wavelength (~0.8µm) GaAs/AlGaAs graded-index separate-confinement heterostructure quantum-well laser has been monolithically integrated with a long-wavelength (~8µm) GaAs/AlGaAs multiple-quantum-well infra-red photodetector on a semi-insulating GaAs substrate by molecular beam epitaxy. The vertical integration method is used and the combined structure is a *pinin* structure. Both the laser and detector exhibit excellent characteristics. At room temperature, the ridge waveguide laser has an extremely low threshold current of 25mA and a differential quantum efficiency above 65% with a stripe width of 20µm. The quantum-well detector has a peak response at 8µm and a responsivity of 0.7A/W.

In recent years there has been continuous interest in developing optoelectronic integrated circuits (OEICs). This is mainly due to the potential for achieving compact, highly-reliable and multifunctional devices. To integrate different functional devices, the compatibilities of the materials used and the device structures must be considered. Among the various integration techniques, the vertical integration method which stacks two structures one on top of the other is one of the simplest [1, 2]. It does not require the regrowth process which often degrades the quality of the epitaxial layers and has been applied in the integration of a laser with a heterojunction bipolar transistor, a laser with a field-effect transistor and a laser with a photodetectors [2–4]. In previously reported work, the laser and the photodetector integrated as an optoelectronic device are often operates at the same wavelengths [5, 6]. In this Letter we demonstrate for the first time the integration of a short-wavelength (~0.8µm) near-infra-red laser and a long wavelength (~8µm) quatum-well infra-red photodetector (QWIP). This integrated device, for future application, can be used to convert a far-infra-red signal to a near-infra-red (or visible) light signal. The device, which includes a ridge-waveguide laser and a grating-coupled QWIP, is fabricated on a semi-insulating substrate with all the contact electrodes on the front surface.

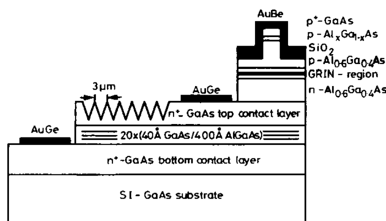

Fig. 1 *Schematic structure of vertical integrated device*

The schematic structure of the integrated device is shown in Fig. 1. The integrated structure contains a graded-index separate-confinement heterostructure (GRINSCH) laser and a quantum-well infra-red photodetector (QWIP). The epilayers were grown by a Varian GEN-II molecular-beam-epitaxy (MBE) system on a (100) semi-insulating GaAs substrate. The first stacked structure was designed as an *nin* QWIP structure. It consisted of a 1.4µm-thick n^+-GaAs bottom-contact layer (Si = $2 \times 10^{18}cm^{-3}$), 20-period GaAs/AlGaAs quantum wells with each period consisting of a 40Å *n*-GaAs quantum well (Si = $1 \times 10^{18}cm^{-3}$) sandwiched between 400Å undoped $Al_{0.26}Ga_{0.74}As$ barriers, and a 1.1µm-thick n^+-GaAs top contact layer (Si = $2 \times 10^{18}cm^{-3}$). The top contact layer of the QWIP was also used as the *n*-type contact layer of the integrated laser. Then, the layers for the laser were grown on top of the n^+-GaAs top contact layer. It consisted of a 1.0µm-thick n^+-$Al_{0.6}Ga_{0.4}As$ cladding layer (Si = $1 \times 10^{18}cm^{-3}$), a 0.15µm-thick undoped $Al_xGa_{1-x}As$ graded-index layer (x = 0.6–0.2), a 65Å GaAs quantum well, a 0.15µm-thick undoped $Al_xGa_{1-x}As$ graded-index layer (x = 0.2–0.6), a 1.0µm-thick *p*-$Al_{0.6}Ga_{0.4}As$ cladding layer (Be = $1 \times 10^{18}cm^{-3}$), a 0.15µm *p*-$Al_xGa_{1-x}As$ graded-index layer (x=0.6-0.2), and a 0.3µm p^+-GaAs ohmic contact layer (Be = $2 \times 10^{18}cm^{-3}$). The whole structure was grown at 580°C with an As_2 source. After MBE growth, the ridge-waveguide pattern was obtained by standard photolithography and wet chemical etching. The width of the stripe was 20µm and the etched depth was about 1.2µm. After chemical etching, a 1500Å SiO_2 layer was deposited by plasma-enhanced chemical vapour deposition. Contact windows were opened and AuBe was deposited as the *p*-type contact. After *p*-type metallisation, another photolithography step was performed to protect the laser stripe region, and the area not protected was etched away to expose the n^+-GaAs top contact layer of the QWIP. After wet etching, AuGe was deposited and used as the *n*-type contact of the laser. Then, 3µm etched stripe gratings which were used to couple the normal incident infra-red radiation were fabricated on the n^+-GaAs top contact layer by standard photolithography and wet chemical etching. Then another chemical etching step was performed to expose the bottom GaAs layer and AuGe was deposited as the bottom electrode of the QWIP. The substrate was then lapped down to 100µm; devices with a cavity length of 400 µm and a width of 600µm were obtained by cleaving. The widths of all the contact regions were 100µm and the width of the stripe grating region was 200µm.

After the fabrication process, the lasers were measured at room temperature under pulse conditions. The QWIPs were measured with infra-red irradiation from the front side at 77K by the Nicolet Fourier transform infra-red spectrometer. The responsivity of the detector was measured by the standard lock-in technique using a 973K black-body source.

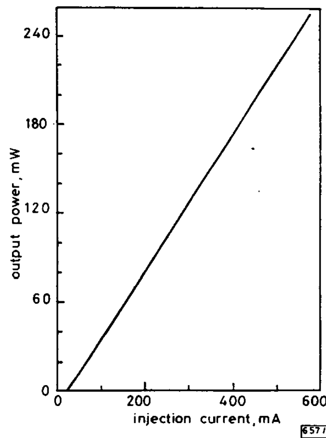

Fig. 2 *Light/current characteristic of an integrated laser*

Threshold current is 25mA and the differential quantum efficiency is above 65%

The light/current characteristic for this integrated GRINSCH laser with a 400µm cavity length is shown in Fig. 2. At room temperature, the threshold current is typically in the 25±2mA range for lasers with uncoated facets. The differential quantum efficiency considering the outputs from both facets is above 65%. Both the threshold current and the quantum efficiency are comparable to those of lasers grown on an n^+-GaAs substrate with the contacts at the front and back sides. The light output had a peak wavelength of 8372Å.

Fig. 3 displays the spectral response of a QWIP device at 77K with a bias voltage of 2V. The peak wavelength of the integrated QWIP is centred around 8µm. The 77K responsivity of the detector at 8µm is 0.7A/W, which is close to the optimum value of the GaAs/AlGaAs QWIPs with the response peak around 8µm [7].

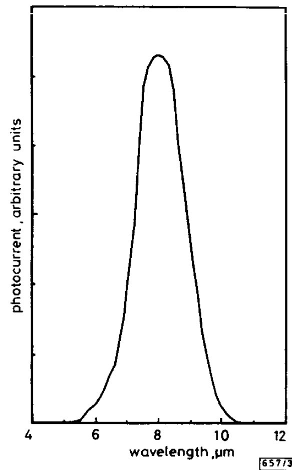

Fig. 3 *Spectral response of integrated QWIP with bias voltage of 2 V at 77 K*

In conclusion, we have successfully used the vertical integration method to integrate a GaAs/AlGaAs GRINSCH quantum-well laser and a GaAs/AlGaAs long-wavelength photodetector by molecular beam epitaxy. The laser's emission wavelength and the photodetector's absorbtion wavelength fall in the near-infra-red and far-infra-red, respectively. The peak wavelength of the laser spectrum is 8372Å at room temperature and the response peak of the QWIP is centred around 8µm at 77K. The typical laser's threshold current is 25mA and the differential quantum efficiency is above 65%. The responsivity of the detector is about 0.7A/W at 8µm.

Acknowledgment: We would like to thank L. J. Cheng for device bonding. This work was supported in part by the National Science Council of the Republic of China under contract NSC82-0404-E009-381.

© IEE 1994
7 January 1994
Electronics Letters Online No: 19940295

J. S. Tsang, C. P. Lee, K. L. Tsai and H. R. Chen (*Department of Electronics Engineering and Institute of Electronics, National Chiao Tung University, Hsin-Chu, 30050, Taiwan, Republic of China*)

References

1 HONDA, Y., SUEMUNE, I., YASUHIRA, N., and YAMANISHI, M.: 'A new optoelectronic device based on modulation-doped heterostructure: Demonstration of functions as both lateral current injection laser and junction field effect transistor', *IEEE Photonics. Technol. Lett.*, 1990, **12**, pp. 881–883

2 CHEN, T.R., UTAKA, K., ZHUANG, Y.H., LIU, Y.Y., and YARIV, A.: 'A vertical monolithical combination of an InGaAsP/InP laser and a heterojunction bipolar transistor', *IEEE J. Quantum Electron.*, 1987, **QE-23**, pp. 919–924

3 OFFSEY, S.D., TASKER, P.J., SCHAFF, W.J., KAPITAN, L., SHEALY, J.R., and EASTMAN, L.F.: 'Vertical integration of an $In_{0.15}Ga_{0.85}As$ modulation doped field effect transistor and GaAs laser grown by molecular beam epitaxy', *Electron. Lett.*, 1990, **26**, pp. 350–351

4 HASNAIN, G., TAI, K., WANG, Y.H., WYNN, J.D., CHOQUETTE, K.D., DUTTA, N.K., and CHO, A.Y.: 'Monolithic integration of photodetector with vertical cavity surface emitting laser', *Electron. Lett.*, 1991, **27**, pp. 1630–1631

5 BLAUVELT, H., BAR-CHAIM, N., FEKETE, D., MARGALIT, S., and YARIV, A.: 'AlGaAs lasers with micro-cleaved mirrors suitable for monolithic integration', *Appl. Phys. Lett.*, 1982, **40**, pp. 289–291

6 NOBUHARA, H., WADA, O., and FUJII, T.: 'GRINSCH SQW laser/photodiode array by improved microcleaved facet process', *Electron. Lett.*, 1985, **21**, pp. 718–719

7 TSAI, K.L., CHANG, K.H., LEE, C.P., HUANG, K.F, TSANG, J.S., and CHEN, H.R.: 'Two color infrared photodetector using GaAs/AlGaAs and strained InGaAs/AlGaAs multiquantum wells', *Appl. Phys. Lett.*, 1993, **62**, pp. 3504–3506

Effective boundary of channel in quasi-two-dimensional simulation of thin-film semiconductor devices

A.A. Barybin and V.V. Perepelovski

Indexing terms: Semiconductor device models, MESFETs, Thin film transistors

An effective boundary between current channels and depletion regions is introduced. The position of this boundary is defined by taking account of the carrier diffusion in the current channel. This gives a correction to the potential determining the depth of depletion without a diffused channel boundary.

Introduction: The quasi-two-dimensional models of MESFETs [1, 2] are based on the assumption of an abrupt boundary between the current channel and depletion region. Quasi-two-dimensional models (QTDMs) have been created with a transition layer between the depletion region and channel [3]. However, the proposed methods allowing for distribution of charge carriers in the transition layer are somewhat artificial. Below, the problem of modelling MESFET-type structures with smooth boundaries between the depletion region and the channel is reduced to an abrupt boundary problem. This will allow use of QTDM equations obtained formerly while assuming a boundary to be abrupt.

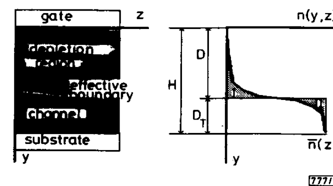

Fig. 1 *Effective boundary of channel-depletion region*

Physical model: The results of MESFET two-dimensional simulation having been analysed, it is possible to use the Boltzmann distribution for free charge carriers in a thin-film semiconductor structure (TFSS) in transverse directions, particularly along the y-axis in Fig. 1 (the z-axis is directed from source to drain):

$$n(y,z) = \bar{n}(z)\exp\{-\varphi_T^{-1}[\varphi(y,z) - \bar{\varphi}(z)]\} \quad \varphi_T = kT_e/q \tag{1}$$

Here $[\varphi(y,z) - \bar{\varphi}(z)]$ is a distribution of the potential in the TFSS cross-section relative to the mean channel potential $\bar{\varphi}(z)$, $\bar{n}(z)$ is the mean carrier concentration in the channel, and $T_e(z)$ is the electron temperature. The mean values $\bar{\varphi}(z)$, $\bar{n}(z)$ etc. are given by averaging over the channel cross-section. We introduce the effective boundary $D(z)$ of a channel by means of the following equality (see Fig. 1):

$$W\int_0^D qn(y,z)\nu(y,z)\,dy = W\int_D^H q[\bar{n}(z) - n(y,z)]\nu(y,z)\,dy \tag{2}$$

where H is the TFSS total thickness, W is the TFSS width along the x-axis, and $\nu(y,z)$ is the electron velocity. The left-hand side of eqn. 2 equals the current flowing in the region confined by the gate (at $y = 0$) and the introduced effective boundary (at $y = D$). This region is denoted by I in Fig. 1. The right-hand side of eqn. 2 corresponds to the region II in Fig. 1 and is written down proceeding from the fact that the current in this region is equivalent